A HIGH-PRECISION EXPLICIT FOREST CARBON STOCK MODEL BASED ON REMOTE SENSING

Ningning Zhu [1], Bisheng Yang [1] *, Weishu Gong [2], Shen Ying [3], Wenxia Dai [4], Zhen Dong [1]

[1] State Key Laboratory of Information Engineering in Surveying, Mapping and Remote Sensing, Wuhan University, Wuhan, Hubei, China - (ningningzhu, bshyang, dongzhenwhu)@whu.edu.cn
[2] Department of Geographical Sciences, University of Maryland, College Park, Maryland, USA - wsgong@umd.edu
[3] School of Resource and Environmental Sciences, Wuhan University, Wuhan, Hubei, China - shy@whu.edu.cn
[4] School of Geography and Information Engineering, China University of Geosciences, Wuhan, Hubei, China – daiwenxia@cug.edu.cn

KEY WORDS: Forest carbon storage, Remote sensing, Forest canopy density, Forest height, Simulated forest.

ABSTRACT:

The current status as well as the potential absorption capability of the forest carbon sinks in terrestrial ecosystems are in urgent need of further studies. The ground observation-based methods are labor-intensive, and the resulting statistics from samples are difficult to evaluate, while inversion methods based on remote sensing data lack theoretical explanation and universality. This paper proposes a pixel-level, multi-scale, high-precision Explicit Forest carbon stock Model (EFM) that is universal and adaptive. First, four key variables were used in the construction of the EFM: remote sensing image resolution, forest canopy density, terrain slope, and forest height; Second, simulated forest scene were generated based on the growth characteristics of individual trees, and EFM parameters were solved and analyzed by these simulated pixels; Third, the EFM was tested at various scales and forest saturation levels to verify its accuracy, robustness, and applicability, the simulation and real-life experiments show that the correlation coefficient is greater than 0.98 and the relative error is about 20%. The EFM solves the problem that the existing methods are lack in theoretical interpretation and universal applicability, thus can be used to map forest carbon stocks at high resolution and large scale and even monitor forest carbon dynamics at global scale.

* Bisheng Yang, bshyang@whu.edu.cn

1. INTRODUCTION

Close monitoring of carbon sinks is critical to researching global climate change, and the current status as well as the potential absorption capability of the carbon sinks in terrestrial ecosystems are in urgent need of further studies(Ding, 2021). Forests, grasslands, shrubs, crops, and soil are the main carbon pools in terrestrial ecosystems(Fang et al., 2007). The United Nations Food and Agriculture Organization (FAO) pointed out that globally, the carbon stocks of forests account for about 77% of the total carbon stocks in vegetation, making them the most important carbon pool in terrestrial ecosystems(FAO, 2021). However, there are significant differences in current estimations of forest carbon sinks based on inventory (Jiang et al., 2016; Fang et al.,2018; Piao et al., 2009), modeling (He et al., 2019; Tian et al.,2011; Friedlingstein et al.,2020), and atmospheric inversion methods (Chen et al., 2021; Zhang et al.,2014; Wang et al., 2020; Schuh et al., 2022). The issue of how to achieve reliable monitoring of global forest carbon sinks is of great urgency (Piao et al., 2022a; Piao et al.,2022b; Fang et al., 2021; Wang, Y. et al., 2022; Wang, J. et al., 2022). With the increasing refinement of satellite remote sensing images in space, time, and spectral domains (Frantz et al., 2020; Li et al.,2020; Potapov et al., 2021), the growing number of satellite laser data acquisition platforms (Bauer et al., 2021; Magruder et al., 2021; Narine et al., 2019; Neuenschwander et al., 2018), and the launching of numerous SAR sensors for forestry and ecological monitoring missions (Leonardo et al., 2020; Lu et al., 2021; Pourshamsi et al., 2020; Tan et al., 2020), using spectral information from satellite remote sensing images and vertical forest structure information from airborne/spaceborne LiDAR (Xu et al., 2021; Bruggisser et al., 2020; Fu et al., 2021; Næsset, 2002), in a combination of ground observation data to monitor the dynamics of global/regional forest carbon sinks has become a hot topic (Duncanson et al., 2021; Guerra-Hernández et al., 2021; Lin et al., 2020; Silva et al., 2020).

For ground observation-based methods, individual tree parameters such as diameter at breast height and tree height are mostly collected under the canopy, which can be used to build tree-level carbon stock model (Zhou et al., 2018; Fang et al., 2022), obtain forest carbon stock at plot-level, and then estimate large scale forest carbon stock using statistical methods (Jiang et al., 2020; Kankare et al.,2013a; Kankare et al., 2013b). This type of method is affected by the number and spatial distribution of sample plots (there are about 200,000 permanent and temporary forest plots in China), the required labor is intensive and the estimation accuracy is difficult to evaluate. For remote sensing-based methods, the spectral and vertical structure information of forests can be collected above the canopy, which reflects the height and coverage of forests at pixel-level, allowing carbon stock mapping with continuous spatial distribution and strong timeliness(Li et al., 2020; Narine et al., 2019). The pixel-level carbon stock estimation is realized by establishing a regression relationship (random forests, deep learning) between the carbon stock of forest sample plots and the characteristics of multi-source remote sensing data. Such methods can overcome the defect of low efficiency of ground observations, their accuracy depends on the selection of independent variables (Potapov et al., 2021; Silva et al., 2021; Liu et al., 2019). However, forced regression models between different variables and forest carbon stock by machine/deep learning are lacking in interpretability and universal applicability.

Current methods have achieved robust performance in the test areas, the models derived from these algorithms are usually difficult to interpret. The patterns or potential relationships between the remote sensing variables and AGB/carbon stock are still unclear. There is no stable and explicit relationship in these models and would lower confidence when these models are applied to other areas (Lu et al., 2016). How to use pixel-level surface and elevation information of forests to establish a multi-scale, interpretable, and high-precision forest carbon stock model is a key scientific issue. This paper proposes an explicit forest carbon stock model (EFM) with solid theoretical explanation. The EFM is suitable for remote sensing images with different spatial resolutions and different forest saturation levels. The solution of the EFM requires a lot of plot data, manually measure variables of different tree species is time-consuming and labor-intensive, simulated forest scenes were constructed based on the growth characteristics of individual trees, and the EFM parameters were solved theoretically.

2. METHODS AND MATERIALS

2.1 The formulation and advantages of EFM

In order to build an interpretable and precision controllable forest carbon stock calculation method, the power function multiplication form of diameter at breast height (D) and tree height (H) adopted by the tree-level carbon stock model is referenced. It is written as $C = c_1 \cdot D^{c_2} \cdot H^{c_3}$, with D and H representing the surface and elevation information of individual tree, respectively. The EFM is shown in Equation (1),which uses the resolution P, forest canopy density F, terrain slope θ, and forest height H of each pixel to express carbon stock C explicitly.

$$C = a \cdot (P^2 F/cos\theta)^b \cdot H^c \quad (1)$$

It is theoretically intepretable to express C as the product of tree species density (a), forest area ($S = P^2 F/\cos\theta$), and elevation (H), therefore, carbon stock in different periods can be calculated simply and quickly, and high-resolution dynamic monitoring of large-scale forest carbon sinks can be realized. The EFM centers on H and F variables, and has the following advantages:

① Theoretical interpretability. S and H represent the surface and elevation information of the forest, respectively, a is related to the tree species density, b and c are the correction coefficient of forest surface and elevation, respectively, and a, b, and c were calculated for different tree species;

② Scale inclusiveness. The EFM takes into account the resolution of remote sensing images and is applicable to different spatial scales;

③ Wide applicability. H can be measured by various advanced techniques such as airborne LiDAR, satellite stereo image pairs, InSAR, and GEDI/ICESat2; F can be directly calculated by airborne LiDAR or remote sensing images.

2.2 The solution and error evaluation of EFM

The EFM is in the form of power function multiplication, the variables can be separated by logarithmic transformation, as shown in Equation (2).

$$ln\,C = ln\,a + b \cdot ln\,S + c \cdot ln\,H \quad (2)$$

Let l=ln C, p=ln a, m=ln S, n= ln H, then Equation (2) is converted into:

$$l = p + b \cdot m + c \cdot n \quad (3)$$

Thus, the least squares adjustment is performed, as shown in the following equation.

$$\boldsymbol{X}= (\boldsymbol{B^T B})^{-} \cdot \boldsymbol{B^T L} \tag{4}$$

Where,

$$\boldsymbol{B} = \begin{bmatrix} 1 & m_1 & n_1 \\ 1 & m_2 & n_2 \\ 1 & \cdots & \\ 1 & m_i & n_i \end{bmatrix}_{i\times 3}, \boldsymbol{L} = \begin{bmatrix} l_1 \\ l_2 \\ \cdots \\ l_i \end{bmatrix}_{i\times 1}, \boldsymbol{X} = \begin{bmatrix} p \\ b \\ c \end{bmatrix}_{3\times 1}.$$

By sampling a small number of forest plots at various scales P with known C, F, H, and θ, the above solution method is used to calculate the EFM parameters (a, b, c) for different tree species. Then, remote sensing images, SRTM, forest height, and other data are used to estimate the forest carbon stock, thus the monitoring of forest carbon sinks dynamics is realized by utilizing data from multiple time periods.

In order to analyze the influence of variable errors on forest carbon stock estimation in EFM, the differentials of F and H are shown in Equation (5).

$$\begin{cases} \frac{d_C}{d_F} = a \cdot (P^2/cos\theta)^b \cdot b \cdot F^{b-1} \cdot H^c = C \cdot b/F \\ \frac{d_C}{d_H} = a \cdot S^b \cdot c \cdot H^{c-1} = C \cdot c/H \end{cases} \tag{5}$$

In order to analyze the influence of parameter errors on forest carbon stock estimation in EFM, the differentials of a, b, and c are shown in Equation (6).

$$\begin{cases} \frac{d_C}{d_a} = S^b \cdot H^c = C/a \\ \frac{d_C}{d_b} = a \cdot S^b \cdot H^c \cdot lnS = C \cdot ln\, S \\ \frac{d_C}{d_c} = a \cdot S^b \cdot H^c \cdot lnH = C \cdot InH \end{cases} \tag{6}$$

Therefore, the variable error (d_F, d_H) equation of EFM can be expressed as:

$$d_C/C = \sqrt{(b \cdot d_F/F)^2 + (c \cdot d_H/H)^2} \tag{7}$$

And the parameter error (d_a, d_b, d_c) equation of EFM can be expressed as:

$$d_C/C = \sqrt{(d_a/a)^2 + (d_b \cdot ln\, S)^2 + (d_c \cdot lnH)^2} \tag{8}$$

2.3 The materials and calculation of EFM

Simulated forest were generated by the growth characteristics and carbon stock model of individual trees at various scales to solve for the EFM parameters. The growth characteristics of individual trees refer to the fixed functional relationship between diameter at breast height (D), tree height (H), and crown diameter (w) of the same tree species (Wang et al., 2022; Li et al.,2010). **Table 1**. and **Figure 1.** list the growth characteristics and tree-level carbon stock models of Chinese fir, pine, and eucalyptus. $H = f(D)$ and $w = f(D)$ represent respectively the functional relationship between H, w, and D; $C = f(D, H) = CF \cdot (W_T + W_R)$ represents the relationship between D, H, and carbon stock of individual trees C, with C equal to the sum of aboveground biomass W_T and underground biomass W_R of individual trees multiplied by the carbon coefficient CF. **Figure 1.** shows H and w of Chinese fir, pine, and eucalyptus under certain values of D.

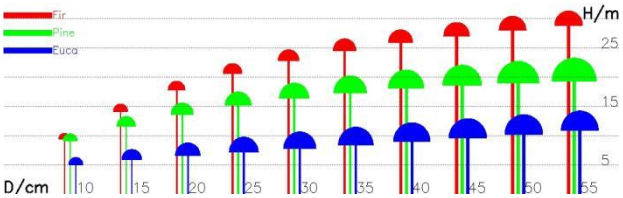

Figure 1. The H and w of different tree species under certain values of D

	$H = f(D)$	$w = f(D)$	$C = f(D,H) = CF \cdot (W_T + W_R)$
Chinese fir	$3.2945 + 1.048\, e^{\left(3.6199 - \frac{18.796}{D+1.0}\right)}$	$1.0974 + 0.1094D - 0.0007D^2$	$\begin{cases} W_S = 0.073429(D^2H)^{0.86262} \\ W_P = 0.013755(D^2H)^{0.84463} \\ W_B = 0.000482(D^2H)^{1.23314} \\ W_L = 0.019638(D^2H)^{0.78969} \end{cases}$ $W_T = W_S + W_P + W_B + W_L$ $W_R = 0.073429(D^2H)^{0.86262}$
Pine	$1.3 + 24.344\,[1 - e^{-0.04D}]^{0.896}$	$0.5290D^{0.674}$	$W_T = 0.071556(D^2H)^{0.857209}$ $W_R = W_T/6.23$
Eucalyptus	$e^{0.73+0.48lnD}$	$0.08803 + 0.27565D - 0.00284D^2$	$\begin{cases} W_S = 0.0902526D^{2.44815} \\ W_B = 0.0049163D^{2.81779} \\ W_L = 0.012694D^{2.26839} \end{cases}$ $W_T = W_S + W_B + W_L$ $W_R = W_T/7.45$

Table 1. The growth characteristics and carbon stock model of individual tree (D in cm; H in m; w in m; C in kg; W_S is the trunk biomass; W_P is the bark biomass; W_B is the branch biomass; W_L is the leaf biomass; W_T is the aboveground biomass; W_R is the underground biomass; CF is the carbon coefficient, a value used for converting biomass into carbon stock , and is generally 0.5).

The EFM are applicable to different spatial resolutions and forest scenes with different saturation levels, the calculation of EFM was divided into the following steps based on the known growth characteristics and carbon stock models of different tree species.

2.3.1 Generating forest pixels

D and the number of trees were set to various values to generate grids with different spatial scales, and forest pixels with various saturation levels were obtained. **Figure 2**(a) shows a 100m×100m area divided into 10m×10m grids, resulting in 100 pixels in total; a single tree with $D \in [5\text{cm}\ 55\text{cm}]$ was randomly set in each grid, H and w were determined by the corresponding growth function. **Figure 2**(b) is the top view of the grids, illustrating the crown in each grid. **Figure 2**(c) shows the panoramic image of the simulated scene in the near ground view. Here, grids at 5 spatial scales were generated, with P = 10m, 20m, 30m, 40m, and 50m, respectively, and each set includes 20×20 = 400 pixels, resulting in a total of 2000 pixels with all 5 scales.

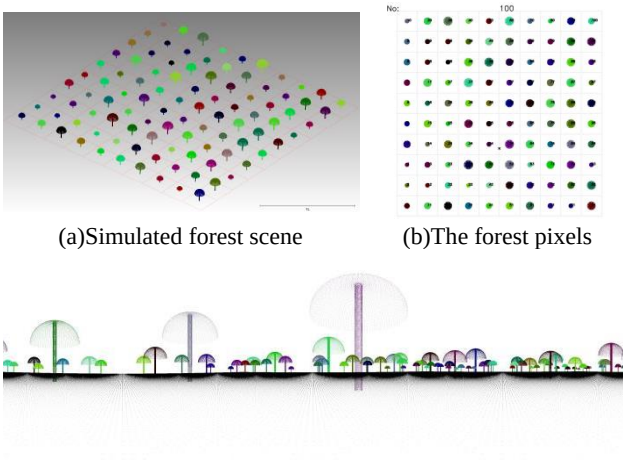

(a)Simulated forest scene (b)The forest pixels

(c)The panoramic image of simulated forest

Figure 2. Generating forest pixels

2.3.2 Calculating *F*, *H*, and *C*

After generating forest pixels with different spatial scales and saturation levels, Equations (9)-(11) were used to calculate the F, H, and C of each forest pixel (θ was set to 0 for all pixels).

$$F = \frac{\sum_{i=1}^{n} S_i}{P^2} \quad (9)$$

$$H = \frac{\sum_{i=1}^{n} h_i S_i}{\sum_{i=1}^{n} S_i} \quad (10)$$

$$C = \sum_{i=1}^{n} \frac{C_i S_i}{\pi (w_i/2)^2} \quad (11)$$

Where P is the resolution of pixel, n is the number of trees in the pixel, w_i is the crown diameter of the ith tree, S_i is the area of w_i within the pixel, h_i is the height of the ith tree, C_i is the carbon stock of the ith tree.

F is the ratio of the forest canopy within the pixel to the pixel area; if the tree canopy is completely within the pixel, then $S_i = \pi(w_i/2)^2$, otherwise, S_i equals the area of tree canopy within the pixel. H is the average height of the forest within the pixel; the height of each tree was considered as h_i wherever covered by its canopy, and the average height of the forest within the pixel was calculated. C is related to the canopy area within the pixel; C_i was evenly distributed in the canopy coverage area $\pi(w_i/2)^2$, and multiplied by S_i to obtain the accurate carbon stock of the pixel.

2.3.3 The calculation of EFM

The F, H, and C of forest pixels at different spatial scales were brought into Equation (2)-(4) to solve EFM parameters a, b, and c. The 2000 pixels at 5 spatial scales were divided equally into two sets, one for training and the other for testing. Taking Chinese fir as an example, **Figure 3**. shows the solutions when F = 0.55, plant density is 500 plants/ha, and carbon stock density is 230.41 Mg/ha.

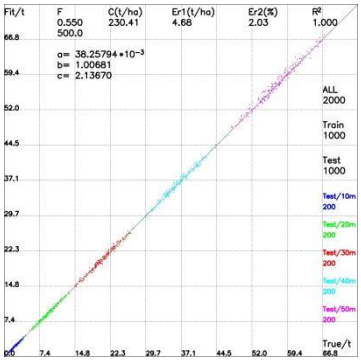

Figure 3. The calculation of EFM

1000 forest pixels were used to calculate the EFM parameters in **Figure 3**, resulting in $a = 38.25794 \times 10^{-3}$, $b = 1.00681$, and $c = 2.1367$. The remaining forest pixels, 200 each for the 5 spatial scales at 10m, 20m,..., and 50m were used to evaluate the model accuracy. In the figure, points with different colors represent the true values (horizontal axis, true) and calculated values (vertical axis, Fit) of forest pixels at different spatial scales. The correlation coefficient $R^2 = 1.000$ based on the 1000 test pixels, Er1 and Er2 were used to quantitatively evaluate EFM errors, and the calculation method is shown in Equation (12).

$$\begin{cases} Er1 = \frac{\sum_{i=1}^{n} |C_i - C_i'| / (P_i/100)^2}{n} \\ Er2 = \frac{\sum_{i=1}^{n} |C_i - C_i'|}{\sum_{i=1}^{n} C_i} \cdot 100\% \end{cases}, C_i' = a \cdot (P_i^2 F_i / cos\theta)^b \cdot H_i^c \quad (12)$$

Where C_i and C_i' are the true and calculated values of pixel carbon stock and n is the number of pixels.
$Er1$ is the absolute error of EFM, the model error $|C_i - C_i'|$ was divided by the corresponding pixel area (ha) to exclude the influence of spatial scales, thus the unit of $Er1$ calculated at various scales is Mg/ha. $Er2$ is the percentage of $|C_i - C_i'|$ to C_i, representing the relative error of EFM. **Figure 3** shows that $Er1 = 4.68$ Mg$/ha$ and $Er2 = 2.03\%$ when F=0.55, thus, when the carbon stock density is 230.41 Mg/ha, both Er1 and Er2 indicate that EFM has high accuracy.

2.3.4 The parameters and parameter errors

The parameters a, b, and c have slight changes under different forest scenarios, 100 groups of forest pixels with $F \in [0.1\ 5.6]$ were generated, and each group contained pixels at the 5 spatial scales. Thus, 100 groups of a, b, and c were solved, the median of each parameter is highly consistent with the average value, which is taken as the final parameters. Equation (8) is the parameter error equation of EFM, the influence of a, b, and c on carbon stock is d_a/a, $d_b \cdot \ln S$, and $d_c \cdot \ln H$ respectively, where, d_a, d_b, d_c are mean square errors calculated by 100 groups of a, b, and c. The parameters and parameter errors of EFM for Chinese fir, pine, and eucalyptus are shown in **Table 2**.

Tree species	a (10^{-3})	b	c	d_a/a (%)	d_b (%)	d_c (%)
Chinese fir	37.741	1.0	2.155	9.770	0.067	2.950
Pine	59.076	1.0	1.687	2.553	0.012	0.845
Eucalyptus	5.389	1.0	3.278	12.485	0.099	4.949

Table 2. The parameters and parameter errors of EFM

3. EXPERIMENTS

The EFM is tested against simulation and real-life experiments to show that EFM has wide applicability both to pixels at various spatial resolutions and under different forest saturation levels.

3.1 The simulation experiments

3.1.1 The multi-scale experiment

Parameters a, b, and c were obtained by 5 spatial scales and 100 levels of saturation. In order to verify that the parameters are applicable at other spatial scales, forest scenes at 91 spatial scales with P=10m, 11m, 12m,..., 99m and 100m were generated, with each scene containing 30×30 pixels, and F=0.5 in all the scenes. Then, the differences between the EFM values and the true values of all 900 pixels were analyzed, and evaluated with Er1, Er2, and R^2. **Figure 4**. shows the results for Chinese fir, pine, and eucalyptus at P=60m and 90m respectively.

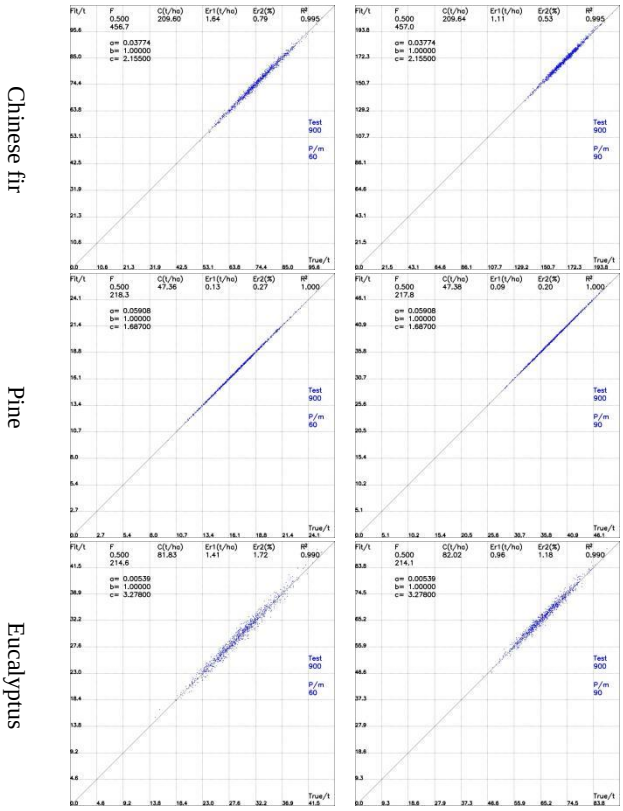

(a) P=60m (b) P=90m

Figure 4. The multi-scale simulation experiments

The EFM values are very close to the true values of the three tree species at P = 60m and 90m, with the minimum R^2 being 0.99, the maximum Er1 being 1.64 Mg/ha, and the maximum Er2 being 1.72%, indicating that EFM is applicable at other spatial scales. The experiment results from 91 scales between 10m to 100m show the EFM is suitable for high-precision calculation of forest carbon stock at multi-spatial scales.

3.1.2 The saturation experiment

Parameters a, b, and c were obtained by averaging the 100 forest scenes with different saturation levels, it is necessary to verify the applicability under other saturation levels. In the above multi-scale applicability analysis, F is uniformly set to 0.5. Here, 600m×600m forest scenes were generated, and F was set to 0.01, 0.02,..., 0.99, and 1.00, then 5 spatial scales, 10m (60×60 pixels), 20m (30×30 pixels), 30m (20×20 pixels), 40m (15×15 pixels), and 50m (12×12 pixels) totaling 5269 pixels were used to analyze the applicability under different saturation levels. **Figure 5**. shows the experiment results of 3 tree species at F = 0.01 and 1.00 respectively.

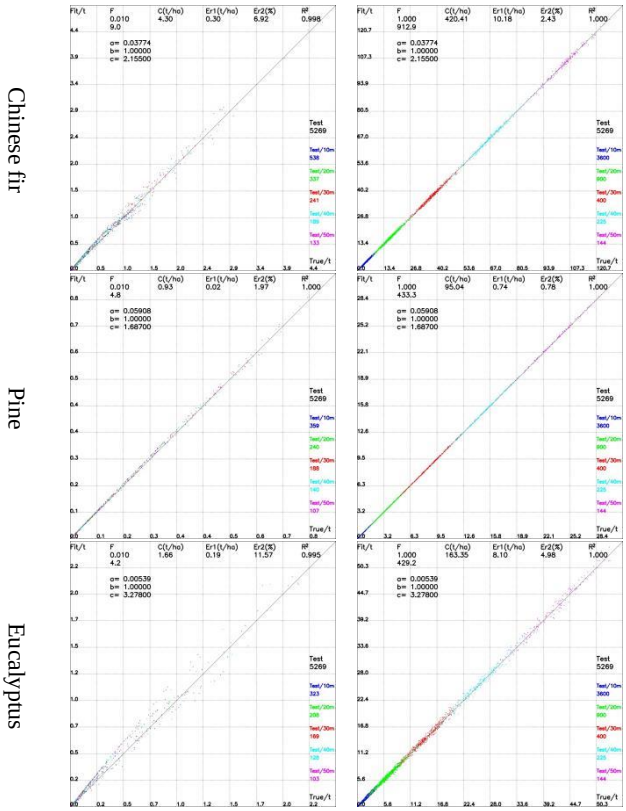

(a) F=0.01 (b) F=1.00

Figure 5. The saturation simulation experiments

The EFM values are highly consistent with the true values of carbon stocks for the three tree species at F=0.01 and F = 1.00, with the minimum R^2 being 0.995, the maximum Er1 being 10.18 Mg/ha, and the maximum Er2 being 11.57%, indicating that EFM is suitable for different saturation levels. The results from 100 different saturation levels, ranging from 0.01 to 1.00, show the EFM is suitable for high-precision calculation of forest carbon stock at any forest saturation level.

3.2 The real-life experiments

The EFM was tested using 2 Chinese fir forests located in Rongshui and Rong'an Counties, Guangxi, China, as shown in **Figure 6**, the whole regions are 1.04km×1.04km, about 108ha, these two blue validation areas are mountainous terrain, the Rongshui validation area is 4.1ha, including 2864 trees, the Rong'an validation area is 4.8ha, including 6029 trees. For each validation area, the D and H of all Chinese firs inside were measured manually, the carbon stock of each tree was calculated using tree-level model (shown in Tab. 1), and the

area total carbon stock was treated as the true value, with C_{True}=394.9Mg and 434.2Mg for each county respectively.

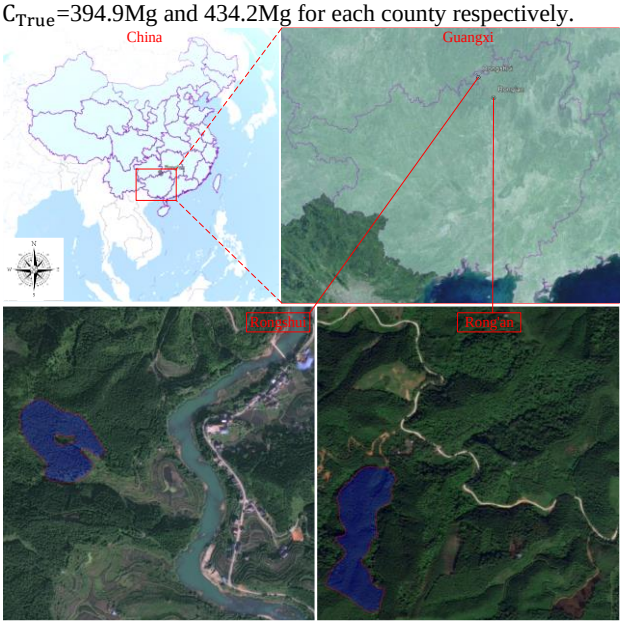

Figure 6. The test area of Rongshui and Rong'an

The airborne LiDAR points in **Figure 7**(a) covering the whole region were used to obtain the DSM and the DEM at 2m resolution, thus H in EFM equals DSM - DEM, θ was calculated from the DEM, and F set to 1.0 because of the high resolution. Then the values of F, θ and H were plugged into the EFM of Chinese fir (**Table 2**.) for pixel-by-pixel calculation, C_{Fit}=357.5Mg and 306.5Mg respectively. Finally, the high-resolution mapping of forest carbon stock was carried out, and the results are shown in **Figure 7**(b); **Table 3**. lists some of the parameters in the experiments of the Rongshui and Rong'an areas.

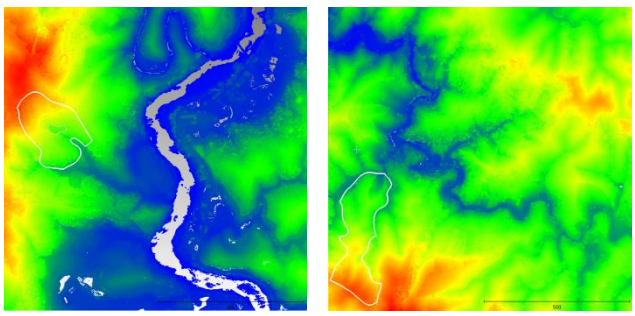

(a) LiDAR points of Rongshui and Rong'an

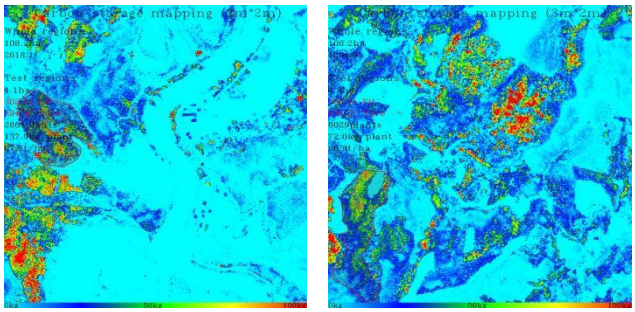

(b) Carbon stock map of Rongshui and Rong'an

Figure 7. Carbon stock maps (resolution: 2m×2m)

Test area	Area (ha)	num	C_{Ture} (Mg)	C_{Fit} (Mg)	δ (%)	C (Mg)	P
Rong shui	4.1	2864	394.9	306.5	22.3	2618	2m
Rong' an	4.8	6029	434.2	357.5	17.6	4294	2m

Table 3. Partial parameters in the experiments

The EFM can rapidly map forest carbon stock with high resolution and accuracy. **Figure 6.** shows the saturation of forests is very high, the current regression method has the problem of oversaturation, EFM is not affected; **Figure 7**(a) shows the airborne LiDAR points, with airborne LiDAR being able to penetrate forest canopies, high-precision DEM and DSM were obtained by filtering the points, then F, θ, and H were calculated with high accuracy. **Figure 7**(b) shows a high precision mapping of forest carbon stock with 2m resolution, and the total carbon stocks are C=2618.1Mg and 4294.9Mg respectively. Then, the accuracy of EFM was verified by manually measuring sample trees in the validation areas. Tab. 3 shows $\delta = 22.3\%$ and 17.6% in Rongshui and Rong'an validation areas, and the theoretical error δ' of Chinese fir can be calculated from Equation (8) and Table 2.

4. CONCLUSION

The current machine/depth learning-based forest carbon stock calculation methods cannot be explained theoretically, have low mapping resolution, and cannot be applied universally. This paper solved such problems by proposing a pixel-level, multi-scale, high precision explicit forest carbon stock model (EFM), deriving forest carbon stocks from four variables: image resolution, forest canopy density, terrain slope, and forest height. The model parameters were solved theoretically from simulated forest scenes, and the results of the experiments showed that the EFM has high accuracy and wide applicability at multiple spatial scales and different forest saturation levels, allowing the monitoring of global forest carbon sinks dynamics. Finally, the EFM is based on the growth characteristics and carbon stock model of individual trees, with the different growth trends of the same tree species in different regions and phenological conditions, the tree-level carbon stock model is differed, constructing EFM according to the growth characteristics and the carbon stock model of individual trees under specific circumstances can improve the accuracy of forest carbon stock calculation.

Acknowledgements: National Natural Science Foundation of China (42101446); China Postdoctoral Science Foundation (2022T150488).

REFERENCES

Bauer, L., Knapp, N., Fischer, R., 2021. Mapping amazon forest productivity by fusing GEDI lidar waveforms with an individual-based forest model. Remote Sens. 13. https://doi.org/10.3390/rs13224540

Bruggisser, M., Hollaus, M., Otepka, J., Pfeifer, N., 2020. Influence of ULS acquisition characteristics on tree stem parameter estimation. ISPRS J. Photogramm. Remote Sens. 168, 28–40. https://doi.org/10.1016/j.isprsjprs.2020.08.002

Chen, B., Zhang, H., Wang, T., Zhang, X., 2021. An atmospheric perspective on the carbon budgets of terrestrial ecosystems in China: progress and challenges. Sci. Bull. 66, 1713–1718. https://doi.org/10.1016/j.scib.2021.05.017

Ding, Z. Research on china's carbon neutralization framework roadmap[R]. Beijing: The 7 annual academic conference of the academic department of the chinese academy of sciences, 2021.

Drake, J.B.; Knox, R.G.; Dubayah, R.O.; Clark, D.B.; Condit, R.; Blair, J.B.; Hofton, M. Above-ground biomass estimation in closed canopy Neotropical forests using lidar remote sensing: Factors affecting the generality of relationships. Glob. Ecol. Biogeogr. 2003,12, 147-159.

Duncanson, L., Kellner, J.R., Armston, J., & Zgraggen, C., 2022. Aboveground biomass density models for NASA's Global Ecosystem Dynamics Investigation (GEDI) lidar mission. Remote Sens. Environ. 270. https://doi.org/10.1016/j.rse.2021.112845

Fang, J., Zhu, J., 2022. Carbon budget of forest ecosystem in china[M]. Beijing: Science Press.

Fang, J., Guo, Z., Piao, S., Chen, A., 2007. Estimation of terrestrial vegetation carbon sink in china from 1981 to 2000[J]. Chinese Science Part D: Earth Science, 37, 804–812.

Fang, J., Yu, G., Liu, L., Hu, S., Stuart Chapin, F., 2018. Climate change, human impacts, and carbon sequestration in China. Proc. Natl. Acad. Sci. U. S. A. 115, 4015–4020. https://doi.org/10.1073/pnas.1700304115

Frantz, D., Schug, F., Okujeni, A., Navacchi, C., Wagner, W., van der Linden, S., Hostert, P., 2021. National-scale mapping of building height using Sentinel-1 and Sentinel-2 time series. Remote Sens. Environ. 252, 112128. https://doi.org/10.1016/j.rse.2020.112128

Friedlingstein, P., O'Sullivan, M., Jones, & Zaehle, S., 2020. Global Carbon Budget 2020. Earth Syst. Sci. Data 12, 3269–3340. https://doi.org/10.5194/essd-12-3269-2020

Food and Agriculture Organization of the United Nations (FAO), 2021. Global Forest Resources Assessment[R]. Rome.

Foody, G.M., Boyd, D.S., Cutler, M.E.J., 2003. Predictive relations of tropical forest biomass from Landsat TM data and their transferability between regions. Remote Sens. Environ. 85, 463-474.

Fu, X., Zhang, Z., Cao, L., Coops, N.C., Goodbody, T.R.H., Liu, H., Shen, X., Wu, X., 2021. Assessment of approaches for monitoring forest structure dynamics using bi-temporal digital aerial photogrammetry point clouds. Remote Sens. Environ. 255, 112300. https://doi.org/10.1016/j.rse.2021.112300

Gou, Y., Ryan, C. M., Reiche, J. 2022. Large Area Aboveground Biomass and Carbon Stock Mapping in Woodlands in Mozambique with L-Band Radar: Improving Accuracy by Accounting for Soil Moisture Effects Using the Water Cloud Model. Remote Sensing, 14(2), 404.

Guerra-Hernández, J., Pascual, A., 2021. Using GEDI lidar data and airborne laser scanning to assess height growth dynamics in fast-growing species: a showcase in Spain. For. Ecosyst. 8. https://doi.org/10.1186/s40663-021-00291-2

He, H., Wang, S., Zhang, Li, Wang, J., Ren, X., Zhou, L., Piao, S., Yan, Hao, Ju, W., Gu, F., Yu, S., Yang, Y., Wang, M., Niu, Z., Ge, R., Yan, Huimin, Huang, M., Zhou, G., Bai, Y., Xie, Z., Tang, Z., Wu, B., Zhang, Leiming, He, N., Wang, Q., Yu, G., 2019. Altered trends in carbon uptake in China's terrestrial ecosystems under the enhanced summer monsoon and warming hiatus. Natl. Sci. Rev. 6, 505–514. https://doi.org/10.1093/nsr/nwz021

Jiang, F., Chen, J.M., Zhou, L., Ju, W., Zhang, H., Machida, T., Ciais, P., Peters, W., Wang, H., Chen, B., Liu, L., Zhang, C., Matsueda, H., Sawa, Y., 2016. A comprehensive estimate of recent carbon sinks in China using both top-down and bottom-up approaches. Sci. Rep. 6, 1–9. https://doi.org/10.1038/srep22130

Jiang, X., Li, G., Lu, D., Chen, E., Wei, X., 2020. Stratification-based forest aboveground biomass estimation in a subtropical region using airborne lidar data. Remote Sens. 12. https://doi.org/10.3390/rs12071101

Kankare, V., Holopainen, M., Vastaranta, M., Puttonen, E., Yu, X., Hyyppä, J., Vaaja, M., Hyyppä, H., Alho, P., 2013a. Individual tree biomass estimation using terrestrial laser scanning. ISPRS J. Photogramm. Remote Sens. 75, 64–75. https://doi.org/10.1016/j.isprsjprs.2012.10.003

Kankare, V., Räty, M., Yu, X., Holopainen, M., Vastaranta, M., Kantola, T., Hyyppä, J., Hyyppä, H., Alho, P., Viitala, R., 2013b. Single tree biomass modelling using airborne laser scanning. ISPRS J. Photogramm. Remote Sens. 85, 66–73. https://doi.org/10.1016/j.isprsjprs.2013.08.008

Karthik, V., Bhaskar, B. V., Ramachandran, S., Gertler, A. W. 2022. Quantification of organic carbon and black carbon emissions, distribution, and carbon variation in diverse vegetative ecosystems across India. Environmental Pollution, 309, 119790.

Leonardo, E.M.C., Watt, M.S., Pearse, G.D., Dash, J.P., Persson, H.J., 2020. Comparison of TanDEM-X InSAR data and high-density ALS for the prediction of forest inventory attributes in plantation forests with steep terrain. Remote Sens. Environ. 246. https://doi.org/10.1016/j.rse.2020.111833

Li, H., Lei, Y., 2010. Assessment of forest vegetation biomass and carbon storage in China. Beijing: China Forestry Publishing House.

Li, Y., Li, M., Li, C., Liu, Z. 2020. Forest aboveground biomass estimation using Landsat 8 and Sentinel-1A data with machine learning algorithms. Scientific reports, 10(1), 1-12.

Li, W., Niu, Z., Shang, R., Qin, Y., Wang, L., Chen, H., 2020. High-resolution mapping of forest canopy height using machine learning by coupling ICESat-2 LiDAR with Sentinel-1, Sentinel-2 and Landsat-8 data. Int. J. Appl. Earth Obs. Geoinf. 92, 102163. https://doi.org/10.1016/j.jag.2020.102163

Lin, X., Xu, M., Cao, C., 2020. Estimates of Forest Canopy Height Using a Combination of ICESat-2 / ATLAS Data and Stereo-Photogrammetry. Remote Sens. 3649.

Liu, Y., Gong, W., Xing, Y., Hu, X., Gong, J., 2019. Estimation of the forest stand mean height and aboveground biomass in Northeast China using SAR Sentinel-1B, multispectral Sentinel-2A, and DEM imagery. ISPRS J. Photogramm. Remote Sens. 151, 277–289. https://doi.org/10.1016/j.isprsjprs.2019.03.016

Lu, H., Zhang, H., Fan, H., Liu, D., Wang, J., Wan, X., Zhao, L., Deng, Y., Zhao, F., Wang, R., 2021. Forest height retrieval using P-band airborne multi-baseline SAR data: A novel phase compensation method. ISPRS J. Photogramm. Remote Sens. 175, 99–118. https://doi.org/10.1016/j.isprsjprs.2021.02.022

Los, S. O. 2013. Analysis of trends in fused AVHRR and MODIS NDVI data for 1982–2006: Indication for a CO2 fertilization effect in global vegetation. Global Biogeochemical Cycles, 27(2), 318-330.

Lu, D., Chen, Q., Wang, G., Liu, L., Li, G., Moran, E. 2016. A survey of remote sensing-based aboveground biomass estimation methods in forest ecosystems. International Journal of Digital Earth, 9(1), 63-105.

Magruder, L., Neuenschwander, A., Klotz, B., 2021. Digital terrain model elevation corrections using space-based imagery and ICESat-2 laser altimetry. Remote Sens. Environ. 264, 112621. https://doi.org/10.1016/j.rse.2021.112621

Narine, L.L., Popescu, S., Neuenschwander, A., Zhou, T., Srinivasan, S., Harbeck, K., 2019. Estimating aboveground biomass and forest canopy cover with simulated ICESat-2 data. Remote Sens. Environ. 224, 1–11. https://doi.org/10.1016/j.rse.2019.01.037

Neuenschwander, A., Pitts, K., 2019. The ATL08 land and vegetation product for the ICESat-2 Mission. Remote Sens. Environ. 221, 247–259. https://doi.org/10.1016/j.rse.2018.11.005

Piao, S., Fang, J., Ciais, P., Peylin, P., Huang, Y., Sitch, S., Wang, T., 2009. The carbon balance of terrestrial ecosystems in China. Nature 458, 1009–1013. https://doi.org/10.1038/nature07944

Piao, S., He, Y., Wang, X., Chen, F., 2022. Carbon sink estimation of terrestrial ecosystems in China: methods, progress and prospects[J]. Chinese Science: Earth Science, 52,1010-1020. https://doi.org/10.1360/sste-2021-0197.

Potapov, P., Li, X., Hernandez-Serna, A., Tyukavina, A., Hansen, M.C., Kommareddy, A., Pickens, A., Turubanova, S., Tang, H., Silva, C.E., Armston, J., Dubayah, R., Blair, J.B., Hofton, M., 2021. Mapping global forest canopy height through integration of GEDI and Landsat data. Remote Sens. Environ. 253. https://doi.org/10.1016/j.rse.2020.112165

Pourshamsi, M., Xia, J., Yokoya, N., Garcia, M., Lavalle, M., Pottier, E., Balzter, H., 2021. Tropical forest canopy height estimation from combined polarimetric SAR and LiDAR using machine-learning. ISPRS J. Photogramm. Remote Sens. 172, 79–94. https://doi.org/10.1016/j.isprsjprs.2020.11.008

Puliti, S., Breidenbach, J., Schumacher, J., Hauglin, M., Klingenberg, T. F., Astrup, R. 2021. Above-ground biomass change estimation using national forest inventory data with Sentinel-2 and Landsat. Remote Sensing of Environment, 265, 112644.

Schuh, A.E., Byrne, B., Jacobson, A.R., Crowell, S.M.R., Deng, F., Baker, D.F., Johnson, M.S., Philip, S., Weir, B., 2022. On the role of atmospheric model transport uncertainty in estimating the Chinese land carbon sink. Nature 603, E13–E14. https://doi.org/10.1038/s41586-021-04258-9

Silva, C.A., Duncanson, L., Hancock, S., Neuenschwander, A., Thomas, N., Hofton, M., Fatoyinbo, L., Simard, M., Marshak, C.Z., Armston, J., Lutchke, S., Dubayah, R., 2021. Fusing simulated GEDI, ICESat-2 and NISAR data for regional aboveground biomass mapping. Remote Sens. Environ. 253, 112234. https://doi.org/10.1016/j.rse.2020.112234

Tan, P., Zhu, J., Fu, H., Wang, C., Liu, Z., Zhang, C., 2020. Sub-canopy topography estimation from TanDEM-X DEM by fusing ALOS-2 PARSAR-2 InSAR coherence and GEDI data. Sensors 20, 1–15. https://doi.org/10.3390/s20247304

Tian, H., Melillo, J., Lu, C., Kicklighter, D., Liu, M., Ren, W., Xu, X., Chen, G., Zhang, C., Pan, S., Liu, J., Running, S., 2011. China's terrestrial carbon balance: Contributions from multiple global change factors. Global Biogeochem. Cycles 25, 1–16. https://doi.org/10.1029/2010GB003838

Vatandaşlar, C., Abdikan, S. 2022. Carbon stock estimation by dual-polarized synthetic aperture radar (SAR) and forest inventory data in a Mediterranean forest landscape. Journal of Forestry Research, 33(3), 827-838.

Wang, J., Feng, L., Palmer, P.I., Liu, Y., Fang, S., Bösch, H., O'Dell, C.W., Tang, X., Yang, D., Liu, L., Xia, C.Z., 2020. Large Chinese land carbon sink estimated from atmospheric carbon dioxide data. Nature 586, 720–723. https://doi.org/10.1038/s41586-020-2849-9

Wang, J., Feng, L., Palmer, PI., Liu, Y., Fang, S., Bosch, H., O'Dell, CW., Tang, X., Yang, D., Liu, L., Xia, C., 2022. Reply to: The size of the land carbon sink in China. Nature, 603, E10-E12.

Wang, X., Zhao, X., 2022. Code for carbon stock survey and carbon source sink data collection of terrestrial ecosystems. Beijing: Science Press.

Wang, Y., Wang, X., Wang, K., Chevallier, F., Zhu, D., Lian, J., He, Y., Tian, H., Li, J., Zhu, J., Jeong, S., Canadell, JG, 2022. The size of the land carbon sink in China. Nature, 603, E7-E9.

Xu, D., Wang, H., Xu, W., Luan, Z., Xu, X., 2021. LiDAR applications to estimate forest biomass at individual tree scale: Opportunities, challenges and future perspectives. Forests 12, 1-19. https://doi.org/10.3390/f12050550

Zhang, X., Brandt, M., Tong, X., Ciais, P., Yue, Y., Xiao, X., ... & Fensholt, R. (2022). A large but transient carbon sink from urbanization and rural depopulation in China. Nature Sustainability, 5(4), 321-328.

Zhou, G., Yin, G., Tang, X., 2018. Carbon Storage of Forest Ecosystem in China--Biomass Equation[M]. Beijing: Science Press.